Am J Transl Res 2018;10(11):3443-3454
www.ajtr.org /ISSN:1943-8141/AJTR0077588

Original Article

Mechanical characterization of 3D printed multi-morphology porous Ti6Al4V scaffolds based on triply periodic minimal surface architectures

Li-Ya Zhu[1,4*], Lan Li[2,3*], Jian-Ping Shi[1,4], Zong-An Li[1,4], Ji-Quan Yang[1,4]

[1]Jiangsu Key Laboratory of 3D Printing Equipment and Manufacturing, Nanjing Normal University, Nanjing 210042, Jiangsu, China; [2]School of Mechanical Engineering, Southeast University, Nanjing 211189, Jiangsu, China; [3]Department of Sports Medicine and Adult Reconstructive Surgery, Drum Tower Hospital Affiliated to Medical School of Nanjing University, Nanjing 210093, Jiangsu, China; [4]Nanjing Institute of Intelligent High-End Equipment Industry Co., Ltd., Nanjing, Jiangsu, China. [*]Equal contributors and co-first authors.

Received April 8, 2018; Accepted October 17, 2018; Epub November 15, 2018; Published November 30, 2018

Abstract: Heterogeneous biomaterials that simultaneously mimic the topological and mechanical properties of nature bone tissues are of great interest in recent years. In this study, multi-morphology porous scaffolds based on the triply periodic minimal surfaces (TPMS) were designed and 3D printed with spatially changing pore patterns. Experiments and numerical analyses were carried out to assess the mechanical properties of the multi-morphology graded porous scaffold. As can be seen from the results, the multi-morphology structure showed a combination of relatively low elastic moduli and high yield strength. This combination allows for simultaneously minimizing the bone damage and increasing the stability of bone-implant interface. Thus the 3D printed multi-morphology porous Ti6AlV scaffold had shown significant promise for orthopedic application.

Keywords: Triply periodic minimal surface, multi-morphology scaffold, graded porous structure, 3D printing, bone tissue engineering

Introduction

In tissue engineering, porous scaffolds could provide a three-dimensional template for cell attachment, proliferation and differentiation [1, 2]. Ideally, the designed scaffold should best mimic the host tissue both biologically and mechanically [3]. Take the bone tissue for example. Accidents, infections, bone tumors and other disease could cause bone defect, making bone repair and regeneration a great challenge [4]. Titanium and some of its alloys have been widely used for bone implants because of their good biocompatibility, high fatigue resistance, corrosion resistance and osseointegration properties. However, the titanium materials show much higher moduli (about 110 GPa) than natural bone (range from 0.5 GPa to 20 GPa) [5]. This moduli mismatch between the implant and its host bone tissue would lead to implant loosening and bone resorption around the metallic implant. This phenomenon is referred as “stress shielding”, which could be avoided by designing porous implants to obtain moduli comparable to the nature hosts [6, 7].

Conventional techniques for the fabrication of porous scaffolds include powder sintering, plasma spray coating and solid-state foaming [8, 9]. However, the pore geometry, pore size and distribution, pore interconnectivity could hardly been controlled with these technologies. With the development of biomaterials and 3D printing technologies, porous scaffolds with controllable porosity and microstructures could be fabricated, which would improve mechanical properties of the implants and enhance their long-term stability and bone in-growth [10-12]. Selective laser melting (SLM), as one of these 3D printing methods, are capable of fabricating porous scaffolds with titanium materials directly from computer-aided design models [13, 14]. However, majority of existing titanium scaffolds are designed on the basis of cubic lattices with straight edges and sharp turns which would not be suitable for cell attachment, migration and proliferation [3]. Moreover, it would be difficult

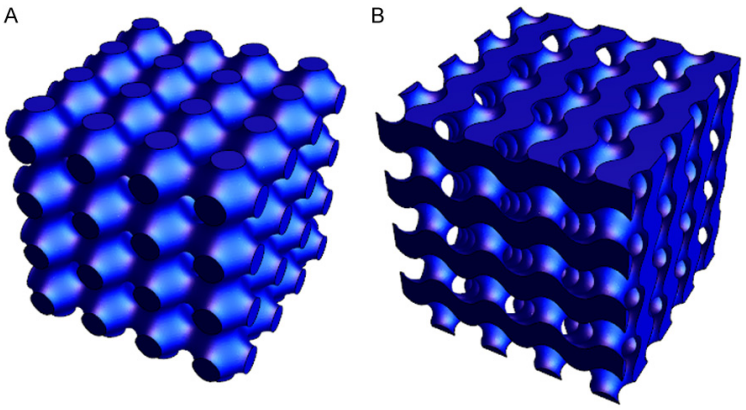

Figure 1. Some of the basic mathematically defined TPMS structure types: (A) Primitive, (B) Gyroid.

to fabricate such scaffolds with SLM technique in large unit cell sized as a result of thermal deformation [15].

Triply periodic minimal surfaces (TPMS) have emerged as a promising tool for designing porous scaffolds with smooth joints and are periodic in three independent directions. Recent research studies on TPMS based scaffolds have shown that these scaffolds could provide better mechanical and biological properties compared to the traditional scaffolds composed of rod connected porous structures. Furthermore, pore architectures of TPMS based scaffolds could be arranged from macro-scale to nana-scale according to biological properties of native tissues [16-19]. Yoo et al. proposed scaffolds composed of multiple TPMS morphologies and arbitrarily-shaped transition boundaries within one scaffold [20]. Yang et al. also investigated an improved combination operations of multiple substructures that could be easily constructed and fabricated [21]. Yan et al. investigate the manufacturability, microstructure and properties of titanium alloy TPMS structures fabricated by SLM [3]. Bobbert et al. designed porous metallic biomaterials based on four different types of TPMS and then characterized the mechanical properties, fatigue resistance and permeability of the developed biomaterials to mimic the properties of bone [22].

Despite numerous studies about TPMS-based scaffold had been conducted, to date, few work explored the mechanical characterization of multi-morphology graded porous scaffolds combining different TPMS pore architectures. However, many nature tissues exhibits a heterogeneous material and structure distribution. For example, a femur has a dense cortical shell, a porous cancellous interior, and a transition boundary that is approximately a cylinder surface [19, 20]. Thus the bottom layer of the scaffold is expected to mechanically match the cortical bone while the top layer should be close to the cancellous bone with gradient porosity. Therefore, how mechanical properties for regular TPMS dominated porous structure could be controlled by considering a combination of different TPMS morphologies were studied in this paper. To achieve this goal, mathematical models of graded porous scaffold composed of varying TPMS units was established; then the effective moduli of such graded structure was studied using finite element analysis (FEA) to investigate its mechanical properties. For validation, samples were manufactured using SLM technology and mechanically tested eventually.

Materials and methods

Scaffold modeling based on TPMS architectures

As shown in **Figure 1**, two basic porous TPMS structures, known as P and G surfaces are considered in this paper. Based on the previous researches [16, 23], these porous structures could be represented by the following functions.

Primitive (type P) TPMS:

$$\phi_P(x,y,z) = \cos(ax) + \cos(by) + \cos(cz) + d \quad (1)$$

Gyroid (type G) TPMS:

$$\phi_G(x,y,z) = \cos(ax)\sin(by) + \cos(by)\sin(cz) + \cos(cz)\sin(ax) + d \quad (2)$$

The pore size and surface architectures are controlled by the parameters *a*, *b* and *c* in the above functions. Porosity can be varied by the

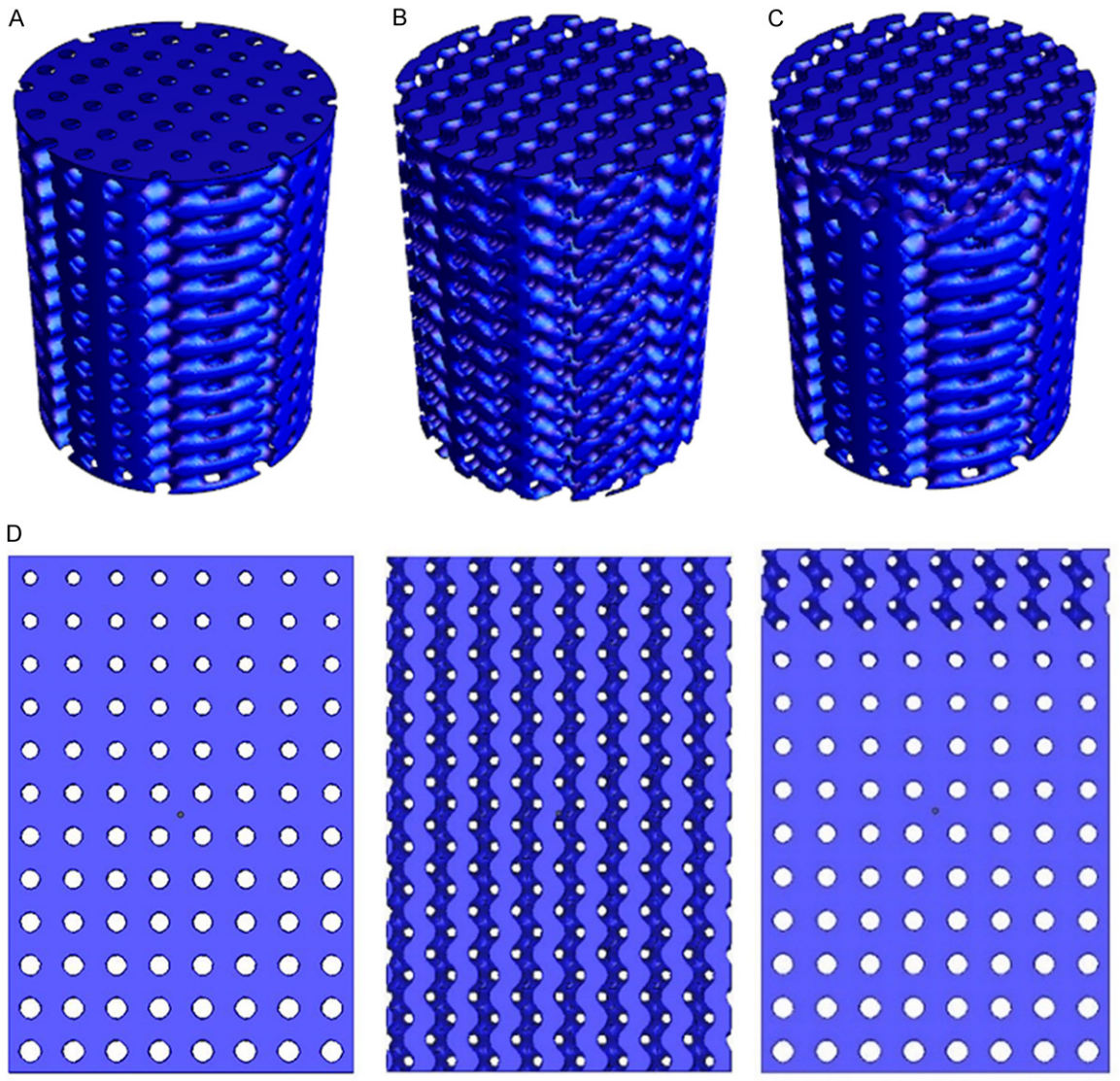

Figure 2. Scaffold modeling: (A) Graded porous structure based on P surface, (B) Porous structure based on G surface, (C) Multi-morphology graded porous structure combing P and G surfaces, (D) Side view of these scaffold models.

Table 1. Chemical component of Ti6Al4V (mass faction %)

Materials	Ti	Al	V	C	Fe	O	N	H
Content	Bal	6.04	4.05	0.01	0.07	0.13	0.005	0.005

parameter d [19]. Meanwhile, an area of $\Phi \geq 0$ represents the solids, and $\Phi < 0$ represents the pores.

As for graded scaffolds designed in this study, the offset value of d in type P TPMS was defined as a linear function of scaffold height in order to obtain the graded structure:

$$\phi_P(x,y,z) = \cos(ax) + \cos(by) + \cos(cz) + kz \quad (3)$$

Then there should be a smoothly connect between the graded type P and the periodically type G TPMS morphologies to obtain a multi-morphology graded porous structure. The whole structure can be generated by one sigmoid function (SF) operation, defined as:

$$\phi_{wh}(x,y,z) = \frac{1}{1+e^{-k\phi_b(x,y,z)}}\phi_G(x,y,z) + \frac{1}{1+e^{k\phi_b(x,y,z)}}\phi_P(x,y,z) \quad (4)$$

where Φ_{wh} indicates the function of the whole multi-morphology and $\Phi_b(x,y,z) = 0$ is the transi-

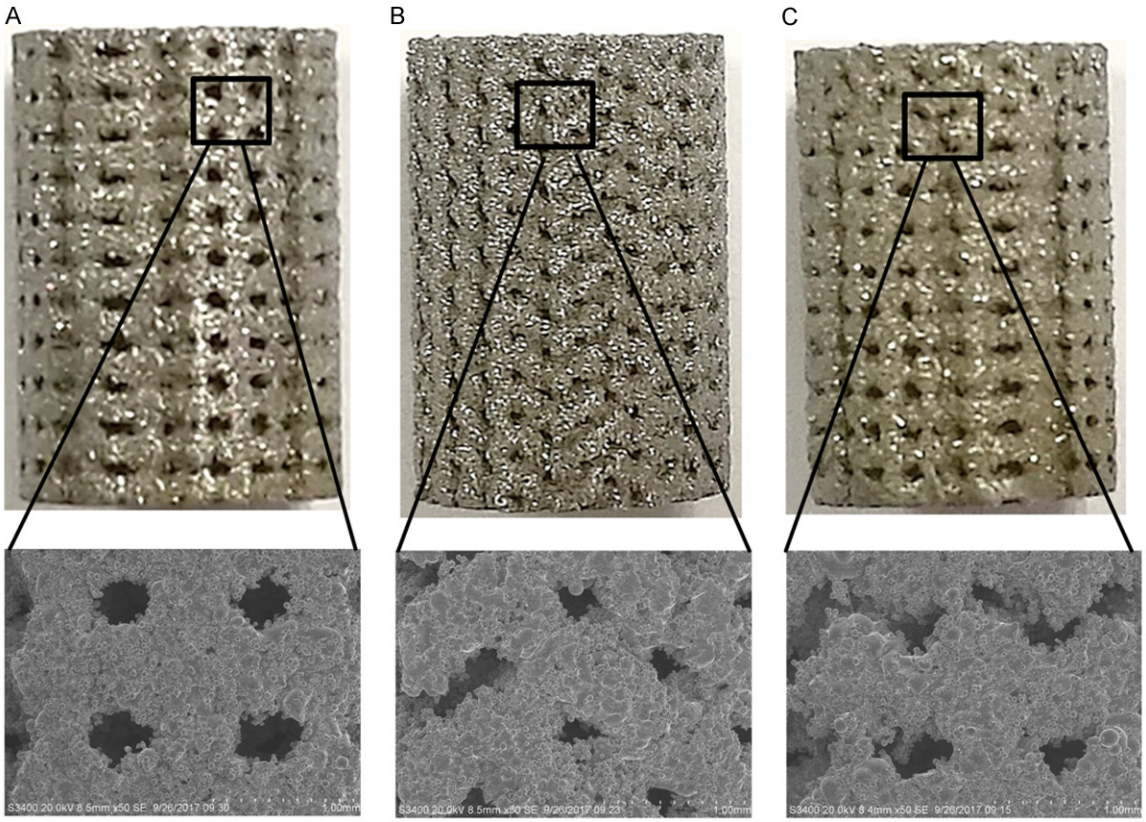

Figure 3. Appearance and SEM images (×50) of the printed scaffolds: (A) Graded structure based on P surface, (B) Porous structure based on G surface, (C) Multi-morphology graded structure combing P and G surfaces

tion boundary between two pore morphologies, and k determines the transition gradient.

Moreover, it is necessary to combine the designed graded porous structure with a given external shape for different applications [24]. Here we attempted to construct a simple cylinder external shape for further in vivo experiment. The model was defined by the Boolean set expression as follows:

$$\begin{aligned} &S_1 \cap S_2 \\ &S_1 = (\phi_{ex} \leq 0) \\ &S_2 = (\phi_{wh} > 0) \\ &\phi_{ex} = x^2 + y^2 - r^2 \end{aligned} \tag{5}$$

where r is the radii of cylinder. The resulting modes were constructed and then exported as STL file using Wolfram Mathematica 11.0 software, as shown in **Figure 2**.

Materials and fabrication

The Ti6Al4V power (particle size of 45~100 μm, a nominal composition shown in **Table 1**) was purchased from Electro Optical System (EOS) GmbH, Germany. The power exhibits a nearly spherical shape and smooth surfaces, indicating a good flowability. The TPMS morphology based cylindrical specimens with a designed height of 12 mm and a diameter of 8 mm were fabricated using DMLS EOSINT-M290 Machine supplied by EOS GmbH, Germany (**Figure 3A**). The processing parameters were chosen as: the laser power of 380 W, the scanning speed of 400 mm/s, the spot size of 100 μm, the 0.1% oxygen content, the layer thickness of 20 μm and the hatch spacing of 60 μm. The as-built samples were post-processed with a thermal stress-relieving heat treatment cycle in an argon atmosphere. Finally, the Ti6Al4V porous structures were obtained by the removal from the base plate. The microstructure, pore size and pore morphology of the manufactured porous Ti6Al4V scaffolds were visualized using SEM (S3400, HITACHI). The porosity of these samples was determined using the gravimetric method [25].

Mechanical compressive test

To obtain the mechanical response of the manufactured scaffolds, compressive tests were

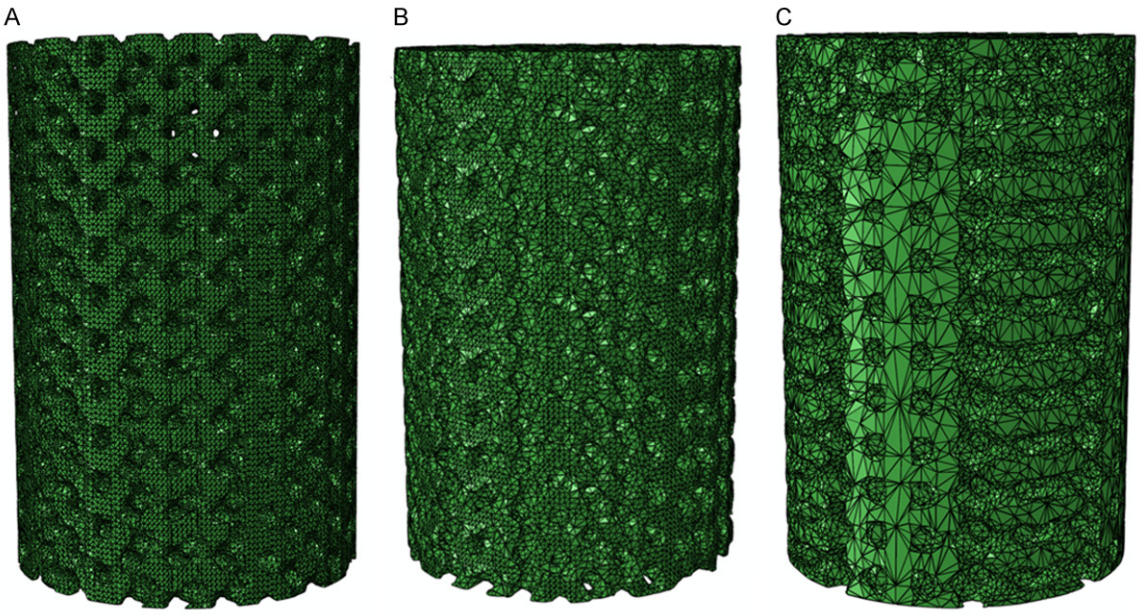

Figure 4. Voxel mesh used for FE simulating: (A) Graded structure based on P surface, (B) Porous structure based on G surface, (C) Multi-morphology graded structure combing P and G surfaces.

carried out using an Electro-mechanical Universal Testing Machine (CTM5105) equipped with 10 kN load cell. Mechanical compressive tests were implemented with 1 mm/min head speed while displacements were correspondingly measured by deflectometer or compressometer. Apparent stress was obtained by dividing the compressive force into initial cross-sectional area of the samples and strain values were calculated by dividing displacement into the initial length of scaffolds. Consequently, the stress-strain curves were obtained and the elastic modulus of these porous scaffolds could be determined from the linear region of those curves. And the yield stress could be found by the intersection of the stress-strain curve and a line parallel to the quasi-elastic gradient line at a strain offset of 0.2% [26]. Furthermore, images were taken to illustrate the state of microstructure after failure.

Computational simulation procedure

The 3D finite element (FE) analysis was conducted using the ABAQUS/CAE software in order to validate numerical stress-strain behavior with the experimental results. The proposed porous scaffolds were modelled using solid tetrahedral elements with a global seeding size of 0.05 mm to allow for small holes or regions of high curvature, as shown in **Figure 4**. The number of body units in the model ranged from 852032 to 1604573. For the numerical computation, a compressive displacement was applied on the top of the models with the strain rate matching the experimental tests. The opposite face of the models were constrained without any displacement. The elastic modulus and the Poisson's ratio of the Ti6Al4V material were set as 110 Gpa and 0.3. Meanwhile, the plastic stresses and strains were defined according to the experimental results obtained by Cain et al. [27]. Finally, the von Mises stress and the apparent elastic modulus of the porous Ti6Al4V scaffolds along the loading direction could be obtained.

Results and discussion

Characterization of 3D printed porous scaffolds

The appearance and surface morphology of Ti6Al4V porous scaffolds observed using SEM were presented with a three dimensional structure (**Figure 3**). It had been shown that the computer-aided 3D-printing method leads to a functionalized scaffold with controlled composition, microstructure and given external shape. The results showed that the porous scaffolds samples had a pore size corresponding with the intended pore size (**Table 2**). Meanwhile, a

Table 2. Mean pore size, Porosity of porous Ti6Al4V scaffolds

			Designed	Manufactured
P surface based structure	Pore size/μm	Top layer	300	320±23
		Medium layer	400	410±17
		Bottom layer	500	480±20
	Porosity/%	Top layer	/	35.8±0.2
		Medium layer	/	51.2±0.6
		Bottom layer	/	60.3±0.4
G surface based structure	Pore size/μm	/	300	280±40
	Porosity/%	/		31.9±0.3
Multi-morphology structure	Pore size/μm	G surface	300	310±35
		P surface (top)	300	305±20
		P surface (Medium)	400	410±25
		P surface (bottom)	500	520±35
	Porosity/%	G surface	/	29.8±0.4
		P surface (top)	/	36.5±0.2
		P surface (Medium)	/	50.4±0.7
		P surface (bottom)	/	61.3±0.6

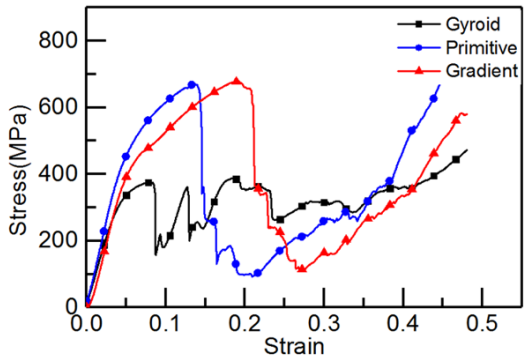

Figure 5. Experimental stress strain curves.

gradient porosity could be seen on the P surface structure and the lower section of the multi-morphology structure (**Figure 3A** and **3C**). The Gyroid section of the multi-morphology structure could be smoothly changed to the graded Primitive section. SEM images showed that the actual pore sized of all 3D printed porous scaffolds presented above were above 300 μm, which was suitable for bone tissue regeneration [22]. Moreover, a highly rough surface could be found for the scaffold surfaces which could provide cells with an environment for attachment, growth and migration along the surfaces.

Experimental results of mechanical tests

The experimental stress strain curves for Ti6Al4V porous scaffolds at 40% volume fractions for the graded P architecture, the G architecture and the multi-morphology graded architecture were presented in **Figure 5**. As can be seen in **Figure 5**, the stress strain curves followed the same trend for these porous structures including a linear increase in stress with strain, a plateau region with fluctuating stresses and finally a rapid increase in stress. Peaks and valleys could be observed due to transformation of build-up stresses to the neighboring porous microstructures. Because of layer by layer collapse of pores, hardening decreased, which lead to a diminishment of slope of stress strain curves as the layers further crushed. Among the curves, the stress strain curve of the Gyroid architectures showed a relatively short yield plateau followed with large levels of irregularity as a result of shear fracture of the porous structure.

Moreover, the mechanical properties extracted from the stress strain curves were presented in **Table 3**. Porous structure based on G surface expressed a relatively lower mechanical properties compared with the others. The mechanical property of the multi-morphology structure was found much closer to the graded P structure rather than the G structure. In general, human cancellous bone has an elastic modulus of less than 3 GPa, and cortical bone has an elastic modulus of less than 20 GPa [5]. In future work, the elastic modulus of the multi-morphology graded porous Ti6Al4V scaffolds would be designed to match that of natural

Table 3. Mechanical properties of 3D printed porous scaffolds based on TPMS

	P surface	G surface	Multi-morphology
Elastic modulus/GPa	9.84±0.03	8.08±0.02	8.18±0.1
Compressive yield stress/MPa	679.2	375.3	670.1

bone by adjusting the morphology region scale and the porosity of different porous morphologies. The multi-morphology graded porous implants could initially provide mechanical stability after being embedded and allow for further vascularization and bone ingrowth. The experimental results verified the validity for repairing large segmental bone defects in load-bearing areas with the proposed graded multi-morphology structures.

Simulation results and model validation

Stress distribution of porous Ti6Al4V scaffolds based on P, G surface and their combination were represented in **Figure 6**. It can be seen that stress concentration was higher in upper layers of graded P structure and showed a gradient decrease layer by layer. The most stress was applied on the vertical struts of the first layer connecting planar layers on each other. The gradient of stress concentration was in accordance with the transformation of pore size. Meanwhile, the compressive stress was equally distributed top-down for the G structure with stress concentration on the struts linking adjacent two layers. The maximum von Mises stresses for the G structure was observed to be larger than the others under the same load pressure, illustrating a lower yield stress. The stress concentration of the multi-morphology structure showed a little decreasement at both top and medium layers compared with that of the porous structure based on P surface only. Furthermore, a smooth transition of stresses could be seen at the connection between the P surface and the G surface. The mechanical properties observed from the simulation results indicated good agreement with that can be seen from the experimental data.

Relationship between porous scaffold structure and stress distribution

The biomechanical effect of the bone-implant interface is one of the most important factors for bone healing. Loads causing strain bearing on bones generate signals that cells can detect and respond. Signals within genetically determined threshold would help to modeling and remodeling. When strains exceed bone's modeling threshold range, modeling would turn to strengthen a load-bearing bone, whereas when strains stay below the lower bone's modeling threshold range, disuse-mode remodeling would turn to reduce bone strength [28]. Thus the strains suffered by the bone should satisfy the typical strain range of load-bearing bones.

The aim of this part was to discuss the effect of the pore patterns of the scaffolds on the stress distribution of the cortical bone. Simplified model of femur bone was built as a cylinder with an inner diameter of 8 mm, an outer diameter of 10 mm and a height of 12 mm by the Magics software. STL models of the femur bone were imported and automatically meshed in ABAQUS, as shown in **Figure 7**. The elastic modulus of the femur bone was set as 7.5 GPa. Porous scaffolds based on the P surface, the G surface and their combing multi-morphology structure were selected as the implants. All materials were assumed to be homogenous, isotropic and linearly elastic. The bone-implant interfaces were assumed to be 100% osseointegrated. The bottom of femur bone were set to be completely constrained, and the boundary conditions were extended to the corresponding node. The physical interactions at bone-implant interfaces during loading were taken into account through bonded surface-to-surface contact features. Static loading was applied to the top of the implanted scaffolds. Since the von Mises stresses were generally considered for heterogeneous objects with more complex mechanical properties, they were used as the key indicators to measure stress levels and evaluate the stress distribution at bone-implant interface, as well as the maximum stress values on femur bone. Under the same loading condition, the stress distributions at the load bearing bone with four different structure implants were compared and analyzed, showing the pore pattern of the implanted structure had significant effects on the stress distribution.

Figure 8 represented the stress distribution at load bearing bone in an axial direction. It can be seen that the structure of the implants had

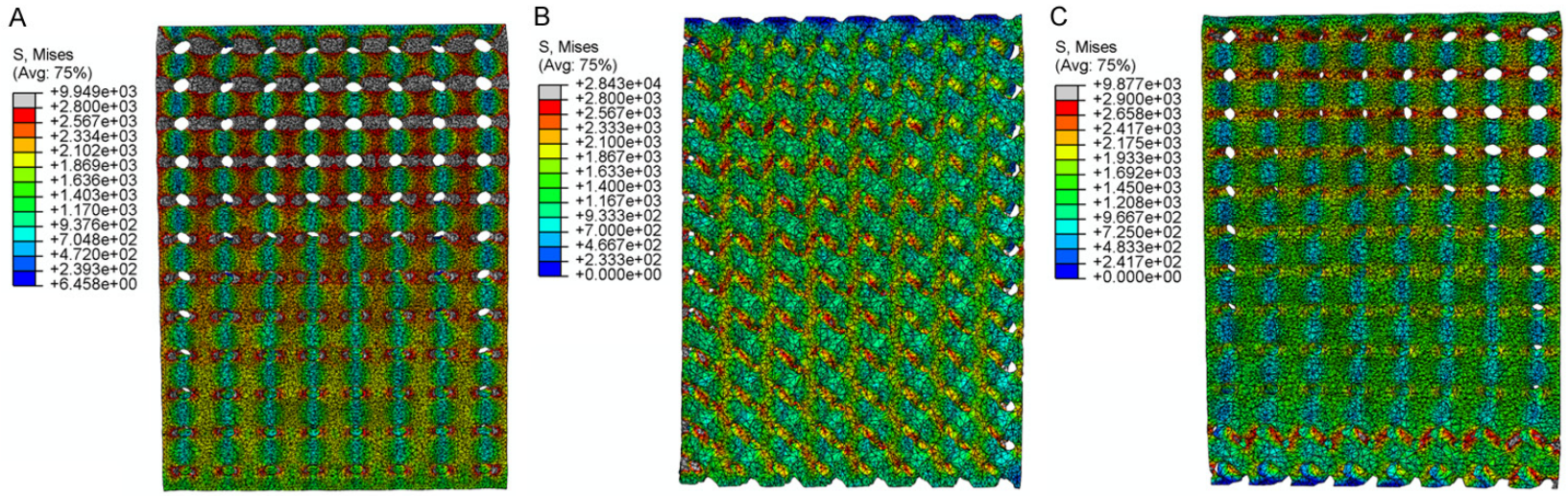

Figure 6. Simulated stress distribution: (A) Graded structure based on P surface, (B) Porous structure based on G surface, (C) Multi-morphology graded structure combing P and G surfaces.

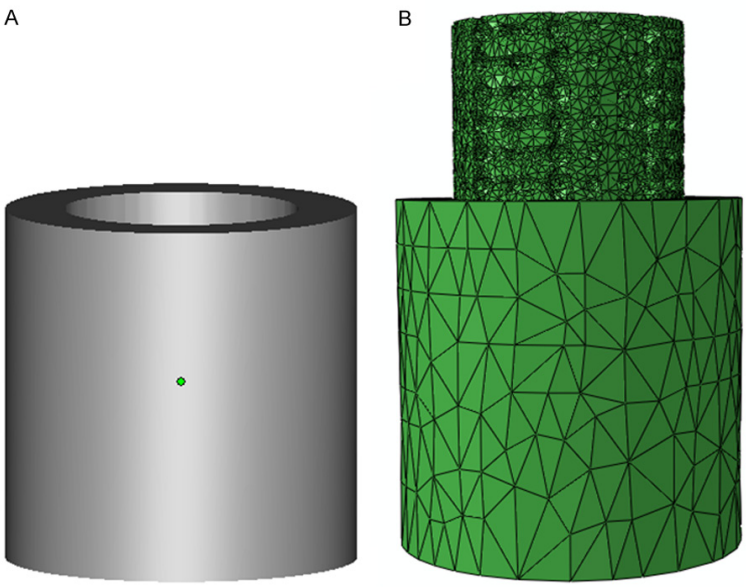

Figure 7. Bone modeling and meshing. (A) Simplified 3D model of femur bone, (B) Mesh of scaffold bone assembly.

a predominate influence on the stress distribution on bones. The stress was concentrated in femur bone under vertical loading in any type of scaffold implants. Furthermore, the stress values increased gradually in the vertical direction. The peak stress varied significantly between the P structure and the others while the change of peak stress was not obvious between the G structure and the multi-morphology structure. The maximum stress on the load bearing bone decreased with the reduction of elastic modulus of the implanted scaffold (graded P structure > multi-morphology gradient structure > G structure). From the biomechanical view, a porous scaffold structure like the G structure would be more beneficial to avoiding excessive stress concentrated on the femur bone, resulting a better long time stability of the implanted scaffold. However, stress analyses were conducted under static loading and the mechanical properties of the materials were set as isotropic and linearly elastic, which may not display the actual situation. Therefore further FEA research as well as experimental confirmation would be conducted in the following researches.

Conclusion

In this study, an effective way of establishing graded structure by combination of multiple TPMS based morphologies had been proposed. Taking advantage of the BF method, the pore size and porosity could be well defined and smoothly transited. Through the multi-morphology porous structure, it is possible not only to change the porosity but also vary the pore architecture spatially. Porous Ti6Al4V scaffolds based on different types of triply periodic minimal surfaces with different pore size and porosities were mathematically designed, 3D printed and characterized to evaluate their mechanical properties and suitability for bone tissue engineering. As can be seen from the experimental data, most porous structures expressed mechanical characteristics within the range of human cortical bone. The yield stress in gradient P structure was the highest among the researched porous structures, indicating an ability of bearing more stress and absorbing more energy in elastic area than the others. It could be concluded that if the linking struts of the porous structure were in the loading direction, the ability of energy absorption would be more than those structures having struts oriented with respect to loading direction. Meanwhile, implanted scaffold with the G structure was proved to be more beneficial to avoiding excessive stress concentrated on the femur bone. It could be seen that if the elastic modulus of the implanted porous structure was lowered, the long-term stability of the implants would be improved. Thus the proposed multi-morphology structure, as a combination of relatively low elastic moduli and high yield strength, would be able to minimize the bone damage while increase the stability of bone-implant interface. On the basis of the aforementioned results, the 3D printed porous Ti6AlV scaffold proposed here had shown significant promise for orthopedic application. Biological studies both *in vitro* and *in vivo* would be performed to evaluate their actual bone regeneration performance in the future.

Acknowledgements

This work was supported in part by the National Nature Science Foundation 51705259 and

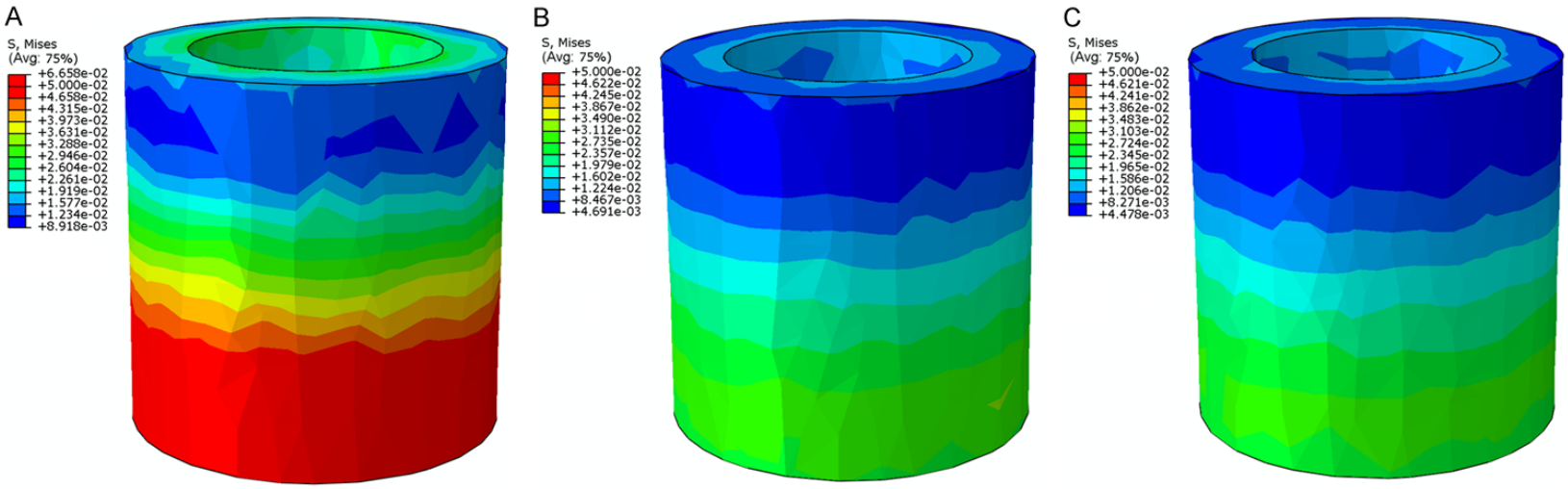

Figure 8. Simulated stress distribution on bone with different porous scaffolds: (A) Gradient structure based on P surface, (B) Porous structure based on G surface, (C) Multi-morphology gradient structure combing P and G surfaces.

51805272, the Natural Science Foundation of Jiangsu Province under Grant BK20150973 and BK20180730, the Key Technology RD Program of Jiangsu Province under Grant BE2016010, the Science and Technology Achievement Transformation Foundation of Jiangsu Province under Grant BA2016106, Scientific Research Foundation of the Higher Education Institutions of Jiangsu Province 18KJB460021, Research funding of Nanjing Normal University 184080H202B135.

Disclosure of conflict of interest

None.

Address correspondence to: Dr. Zong-An Li, School of Electrical and Automation Engineering, Nanjing Normal University, Nanjing 210042, Jiangsu, China. E-mail: ethan301@163.com

References

[1] Martin JR, Gupta MK, Page JM, Yu F, Davidson JM, Guelcher SA and Duvall CL. A porous tissue engineering scaffold selectively degraded by cell-generated reactive oxygen species. Biomaterials 2014; 35: 3766-3776.

[2] Yousefi AM, Hoque ME, Prasad RGSV and Uth N. Current strategies in multiphasic scaffold design for osteochondral tissue engineering: a review. J Biomed Mater Res A 2015; 103: 2460-2481.

[3] Yan C, Liang H, Hussein A and Young P. Ti-6Al-4V triply periodic minimal surface structures for bone implants fabricated via selective laser melting. J Mech Behav Biomed Mater 2015; 51: 61-73.

[4] Li G, Lei W, Wei P, Fei Y, Jiang W, Wu X, Kong X, Dai K and Hao Y. In vitro and in vivo study of additive manufactured porous Ti6Al4V scaffolds for repairing bone defects. Sci Rep 2016; 6: 34072.

[5] Parthasarathy J, Starly B, Raman S and Christensen A. Mechanical evaluation of porous titanium (Ti6Al4V) structures with electron beam melting (EBM). J Mech Behav Biomed Mater 2010; 3: 249-259.

[6] Helguero CG, Amaya JL, Komatsu DE, Pentyala S, Mustahsan V, Ramirez EA and Kao I. Trabecular scaffolds' mechanical properties of bone reconstruction using biomimetic implants. Procedia Cirp 2017; 65: 121-126.

[7] Leong KF, Chua CK, Sudarmadji N and Yeong WY. Engineering functionally graded tissue engineering scaffolds. J Mech Behav Biomed Mater 2008; 1: 140.

[8] Endres S, Wilke M, Knöll P, Frank H, Kratz M and Wilke A. Correlation of in vitro and in vivo results of vacuum plasma sprayed titanium implants with different surface topography. J Mater Sci Mater Med 2008; 19: 1117-1125.

[9] Rouholamin D, Smith PJ and Ghassemieh E. Control of morphological properties of porous biodegradable scaffolds processed by supercritical CO 2 foaming. J Mater Sci 2013; 48: 3254-3263.

[10] Walker JM, Bodamer E, Kleinfehn A, Luo Y, Becker M and Dean D. Design and mechanical characterization of solid and highly porous 3D printed poly(propylene fumarate) scaffolds. Progress in Additive Manufacturing 2017; 2: 99-108.

[11] Senatov FS, Niaza KV, Zadorozhnyy MY, Maksimkin AV, Kaloshkin SD and Estrin YZ. Mechanical properties and shape memory effect of 3D-printed PLA-based porous scaffolds. J Mech Behav Biomed Mater 2016; 57: 139-148.

[12] Giannitelli SM, Accoto D, Trombetta M and Rainer A. Current trends in the design of scaffolds for computer-aided tissue engineering. Acta Biomater 2014; 10: 580-594.

[13] Weißmann V, Bader R, Hansmann H and Laufer N. Influence of the structural orientation on the mechanical properties of selective laser melted Ti6Al4V open-porous scaffolds. Materials & Design 2016; 95: 188-197.

[14] Wang Y, Shen Y, Wang Z, Yang J, Liu N and Huang W. Development of highly porous titanium scaffolds by selective laser melting. Materials Letters 2010; 64: 674-676.

[15] Yan C, Liang H and Raymont D. Evaluations of cellular lattice structures manufactured using selective laser melting. International Journal of Machine Tools & Manufacture 2012; 62: 32-38.

[16] Montazerian H, Davoodi E, Asadi-Eydivand M, Kadkhodapour J and Solati-Hashjin M. Porous scaffold internal architecture design based on minimal surfaces: a compromise between permeability and elastic properties. Materials & Design 2017; 126: 98-114.

[17] Yoo D. Heterogeneous minimal surface porous scaffold design using the distance field and radial basis functions. Med Eng Phys 2012; 34: 625-639.

[18] Afshar M, Anaraki AP, Montazerian H and Kadkhodapour J. Additive manufacturing and mechanical characterization of graded porosity scaffolds designed based on triply periodic minimal surface architectures. J Mech Behav Biomed Mater 2016; 62: 481.

[19] Yang N, Quan Z, Zhang D and Tian Y. Multi-morphology transition hybridization CAD design of minimal surface porous structures for use in tissue engineering. Computer-Aided Design 2014; 56: 11-21.

[20] Yoo DJ and Kim KH. An advanced multi-morphology porous scaffold design method using

volumetric distance field and beta growth function. International Journal of Precision Engineering & Manufacturing 2015; 16: 2021-2032.
[21] Yang N and Zhou K. Effective method for multiscale gradient porous scaffold design and fabrication. Mater Sci Eng C Mater Biol Appl 2014; 43: 502-505.
[22] Fsl B, Lietaert K, Eftekhari AA, Pouran B, Ahmadi SM, Weinans H and Zadpoor AA. Additively manufactured metallic porous biomaterials based on minimal surfaces: a unique combination of topological, mechanical, and mass transport properties. Acta Biomater 2017; 53: 572-584.
[23] Yang N, Tian Y and Zhang D. Novel real function based method to construct heterogeneous porous scaffolds and additive manufacturing for use in medical engineering. Med Eng Phys 2015; 37: 1037-1046.
[24] Yoo DJ. Porous scaffold design using the distance field and triply periodic minimal surface models. Biomaterials 2011; 32: 7741-7754.
[25] Bohner M, van Lenthe GH, Grünenfelder S, Hirsiger W, Evison R and Müller R. Synthesis and characterization of porous beta-tricalcium phosphate blocks. Biomaterials 2005; 26: 6099-6105.
[26] British Standards Institution. Mechanical testing of metals. Ductility testing. Compression test for porous and cellular metals.
[27] Cain V, Thijs L, Humbeeck JV, Hooreweder BV and Knutsen R. Crack propagation and fracture toughness of Ti6Al4V alloy produced by selective laser melting. Additive Manufacturing 2015; 5: 68-76.
[28] Weaver DS. Skeletal tissue mechanics. Springer; 1998.